Hierarchic three-dimensional structure and slip partitioning in the western Dead Sea pull-apart

Amir Sagy, Ze'ev Reches, and Amotz Agnon

Institute of Earth Sciences, Hebrew University, Jerusalem, Israel

Received 20 August 2001; revised 16 July 2002; accepted 1 August 2002; published 20 February 2003.

[1] Rifted basins are bounded by marginal belts with fault networks and flexures. We analyze the internal structure of such a belt, the western margins of the Dead Sea basin. This basin is 150 km long, 15–20 km wide with more than 10 km of sediment fill; and it is currently subsiding due to slip of the Dead Sea pull-apart. The western margin of the Dead Sea basin is an elongated N-S belt with an intricate three-dimensional (3-D) pattern of zigzag faults, flexures and joints. The dominant structures are four sets of oblique-normal faults, arranged in orthorhombic symmetry. The faults are steep with prevalent strike directions of NNW and NNE. Large flexures developed along and above these faults, forming tilted blocks and localized asymmetric folds. Two sets of subvertical joints that dominate the area trend NNE and NNW, subparallel to the strikes of the dominant fault sets. The parallel relations between these structures at all scales suggest that they formed during a single tectonic phase. Three-dimensional fault modeling reveals a 3-D strain field with a large vertical shortening, a minor horizontal shortening in N-S direction (belt-parallel) and a large horizontal E-W extension (basinward). The calculated stress fields associated with the zigzag fault segments are compatible with the observed fault-parallel flexures. Further, the calculations predict the formation of local tensile belts above the faults, and these tensile belts could explain the penecontemporaneous development of the two joint sets. Architecture similar to the western margins of the Dead Sea basin is likely to develop on rifted margins wherever 3-D deformation is required by the rifting kinematics. *INDEX TERMS:* 8105 Tectonophysics: Continental margins and sedimentary basins; 8109 Tectonophysics: Continental tectonics—extensional (0905); 8010 Structural Geology: Fractures and faults; 8020 Structural Geology: Mechanics; *KEYWORDS:* faults, slip partitioning, three-dimensional, pull-apart, joints, zigzag. **Citation:** Sagy, A., Z. Reches, and A. Agnon, Hierarchic three-dimensional structure and slip partitioning in the western Dead Sea pull-apart, *Tectonics*, *22*(1), 1004, doi:10.1029/2001TC001323, 2003.

0278-7407/03/2001TC001323$12.00

1. Introduction

[2] The Dead Sea basin is one of the largest pull-aparts on the Earth with an overall length of 150 km, a width of 15–20 km, and subsidence exceeding 10 km. It developed along a dilational step between two major strike-slip segments of the Dead Sea transform (Arava and Jordan faults; Figure 1) that separates the Sinai-Israel subplate and the Arabian plate [*Quennell*, 1959; *Garfunkel*, 1997]. The elongated Dead Sea basin is bounded by four marginal zones that accommodated its subsidence (Figure 1b). The eastern margins are dominated by dip-slip and strike-slip faults separating the basin from the elevated Arabian plate. The southern transverse margin includes a series of listric, detachment faults [*Arbenz*, 1984], whereas the northern transverse margin flexes gently into the basin [*Katzman et al.*, 1995; *Ginzburg and Ben Avraham*, 1997]. The objective of the present study is the analysis of structural architecture and mechanical evolution of the western margins of the Dead Sea basin.

[3] The western margin of the Dead Sea (WMDS) is a 100 km long and 3–5 km wide belt with cumulative vertical displacement of 10 km or more. We document the three-dimensional (3-D) architecture of this belt and explore the mechanics of its development. The analysis is presented in a hierarchy of four structural scales. First, the regional-scale tectonics is outlined following previous studies. Notably, the internal structure of the WMDS deviates from the regional-scale structures, and could not form under the regional-scale deformation. Second, the zigzag, normal faults are described, and an areal-scale, 3-D strain state is derived to explain their development. Third, flexures and tilted blocks that develop above and along the zigzag faults generated local-scale stresses which induced the formation of the fourth, smallest group of structures dominated by two sets of subvertical joints.

2. Regional-Scale Tectonics

[4] The continental crust in the region of the Dead Sea transform was formed during the Pan-African orogeny of Late Precambrian age, and was later subjected to alternating periods of sedimentation and erosion during the Paleozoic [*Garfunkel*, 1998]. Continental breakup and the establishment of passive margins along the Tethys-Mediterranean coast of the Levant occurred during the Triassic-Jurassic time. From Cretaceous to mid-Eocene, the unbroken African-Arabian plate was a carbonate platform dominated by widespread transgressions. Since the Upper Cretaceous, the region was subjected to WNW compression that created the

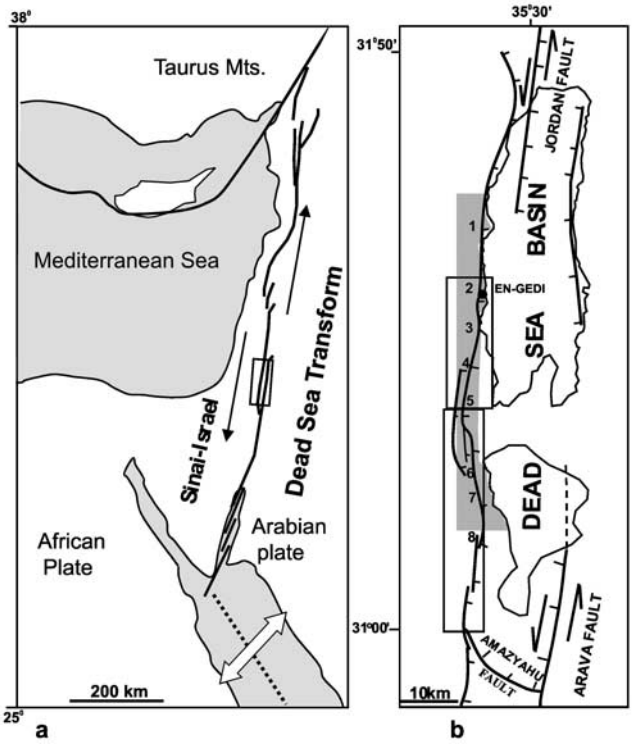

Figure 1. (a) Plate configuration in the eastern Mediterranean; arrows show relative motion along Dead Sea transform and Red Sea; rectangle is enlarged in Figure 1b. (b) The Dead Sea basin and its marginal fault zones. Solid lines- major faults, dashed where inferred; gray zone- study area (western margin of the Dead Sea); numbers- locations of field stations; two rectangular areas are enlarged Figure 2.

1000 km long Syrian-Arc system deforming the sedimentary sequence into a series of asymmetric folds, strike-slip faults, and monoclines [*Eyal and Reches*, 1983]. The African-Arabian plate broke along the suture of Gulf-of-Aden, Red Sea and Dead Sea transform during the Miocene, and this suture has remained the most dominant tectonic feature in the region.

[5] The Dead Sea transform is approximately 1000 km long connecting the oceanic spreading axis of the Red Sea and the continental collision zone at the Taurus Mountains (Figure 1a). The predominant transform motion is left-lateral slip along several major segments inside the transform zone (Figure 1a) [*Garfunkel*, 1981]. The five southern segments, from the northern tip of the Red Sea to southern Lebanon, deviate by a few degrees from the general trend of the transform in a clockwise sense [*Joffe and Garfunkel*, 1986], such that the Dead Sea transform is regarded as a leaky transform [*Garfunkel*, 1981]. The steps between the major segments become pull-apart basins with localized extension normal and parallel to the transform trend [*Garfunkel*, 1981; *Reches*, 1987]. The cumulative slip along the Dead Sea transform is 105 km of left-lateral slip with 10 km (or more) of subsidence in the pull-apart basins [*Garfunkel*, 1997].

[6] The sedimentary cover in the WMDS is at least 3 km thick; Permian rocks were penetrated at 2.5–3.5 km depth (S. Baker et al., unpublished report, 1994). The exposed part of WMDS includes mostly Upper Cretaceous to Paleocene rocks of the Judea and Mount Scopus Groups, respectively with a total thickness of ~700 m [*Agnon*, 1983; *Raz*, 1983; *Mor*, 1987]. The Judea Group sequences include competent limestone and dolomite layers with smaller amounts of marl and shale layers. The Mount Scopus Group contains layered chalk, limestone, chert and marl, and bituminous marls which are the main hydrocarbon source in the basin [*Tannenbaum*, 1983]. The Miocene to Recent sequence includes mostly clastic sediments and evaporites of the Dead Sea Group, and it unconformably overlies the older units. Its thickness varies from more than 10 km in basin center, to a few hundreds of meters close to the WMDS [*Neev and Hall*, 1979].

[7] The intense subsidence and the association of bituminous and clastic layers made the WMDS a promising site for oil exploration [*Tannenbaum*, 1983]. Twenty boreholes were drilled here, including the Sedom-3 borehole to 6445 m depth [*Gardosh et al.*, 1997]. The logging in the Emunah-1 borehole provided direct observations of subsurface fractures that are used in the present analysis.

3. Areal-Scale Architecture: Zigzag, Normal Faults

3.1. General Features

[8] The WMDS was mapped by *Agnon* [1983], *Raz* [1983], and *Mor* [1987], and by E. Aharoni (The surface and subsurface structure of southern Judean Desert, Israel, unpublished report, in Hebrew with English abstract, Hebrew University, Jerusalem, 1978), its subsurface has been studied in seismic profiles and drill holes [*Neev and Hall*, 1979; *Kashai and Croker*, 1987; *Gardosh et al.*, 1997; S. Baker et al., unpublished report, 1994]. The exposed part of the WMDS comprises a series of fault-controlled escarpments with net topographic relief of 300–500 m across the belt. The cumulative throw is generally smaller than the topographic relief with a few exceptions (e.g., ~600 m throw, at location 7, Figure 1b). The mapped length of major fault segments varies from hundreds of meters to a few kilometers. Most faults are down-thrown eastward (basinward), yet antithetic faults are common forming local grabens and horsts [*Agnon*, 1983; *Gardosh et al.*, 1990].

[9] The subsurface part of the WMDS includes large normal faults in the pre-Miocene sequence, underneath the eastward thickening and partly faulted sediments of the Dead Sea Group. The cumulative throw found in boreholes located 500–2500 m east of the exposed part of WMDS is as much as 2.3 km (e.g., En-Gedi-1, En-Gedi-2, and Emunah-1 wells near locations 3, 4 and 5, Figure 1b). This large throw indicates that the subsurface eastern portion of the WMDS accommodates most of subsidence along the margins (>10 km), whereas only ~500 m is accommodated within the exposed part. Some of the major normal faults cut young sediments of the Dead Sea Group [*Agnon*, 1983; *Gardosh et al.*, 1990; *Bartov*, 1999].

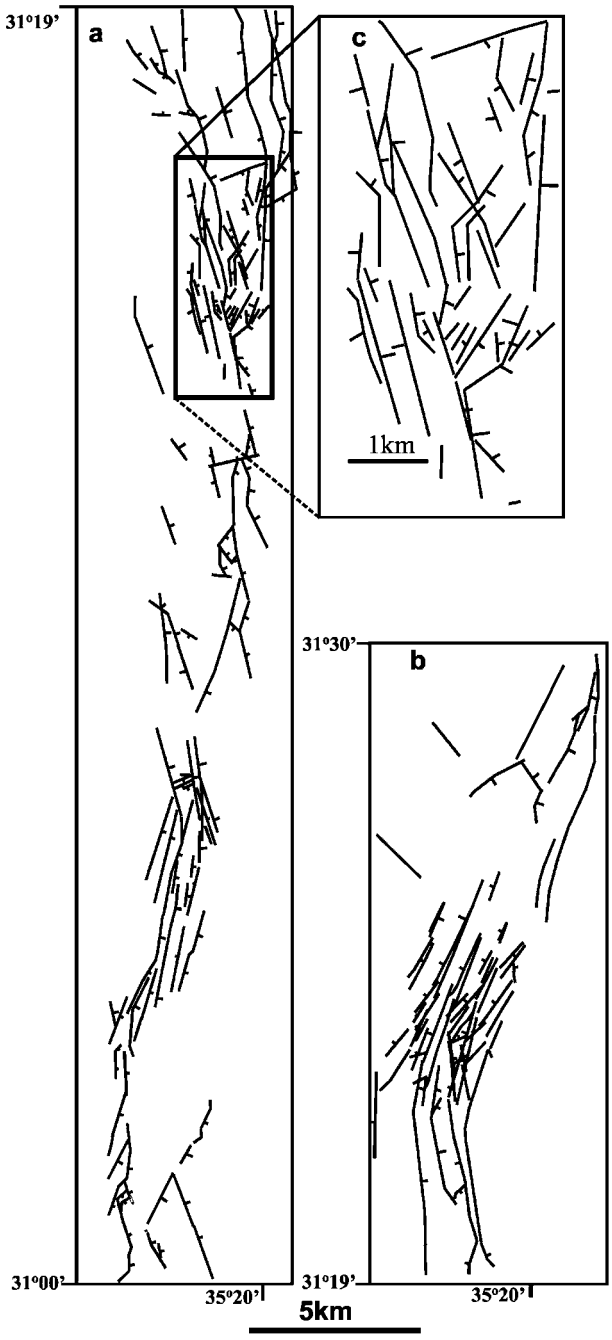

Figure 2. Fault traces in the WMDS digitized from 1:50,000 geological maps of (a) *Agnon* [1983] and (b) *Raz* [1983]. Short bars indicate downthrown side. (c) Enlarged section of Figure 2a. Note zigzag pattern and orthorhombic geometry of the faults.

3.2. Areal Fault Pattern

[10] A casual inspection of the WMDS geologic maps [*Agnon*, 1983; *Raz*, 1983; *Mor*, 1987] reveals a zigzag pattern of faults that are concentrated in a belt with a distinct boundary on its western side (Judean Hills plateau), and a diffusive eastern boundary concealed by the Dead Sea Group (Figure 1b).

[11] We digitized the fault traces on three 1:50,000 geologic maps [*Agnon*, 1983; *Raz*, 1983; *Mor*, 1987], in an 80 km long belt. The cumulative length of the digitized fault traces is 322 km within a 300 km^2 stretch of the WMDS with significant local variations of fault spacing (Figure 2). The faults in the digitized maps are arranged in four sets of subparallel segments that are inclined toward four main directions: ENE, ESE, WNW and WSW (Figure 2). The four fault sets have two major strike directions of 024° ± 15° and 340° ± 16° for the study area (Figure 3). Fault segments of the different sets crosscut each other and interlink along strike forming local blocks of orthorhombic shape (Figure 2c). The sets vary in their relative abundance (Figures 2a and 2b), yet their systematic zigzag links and crosscuts and their areal similarity indicates that the four sets formed during one tectonic episode.

[12] We measured in the field the attitude and slip axes of 38 large faults with throws of tens to hundreds of meters that belong to the zigzag system. These faults are exposed within the carbonate rocks of WMDS. Some of the large fault surfaces display a wavy geometry with strike changes on the scale of 10–50 m; this geometry is a moderate scale appearance of the regional zigzag pattern. The slip axes were determined from slickenside striations and wavy surfaces; if a fault displays multiple slip axes, we used the youngest direction.

[13] The measured faults are oblique-normal with steep inclinations and large directional scatter. We recognized three sets in the field data (Figure 4); the mean values and standard deviations (Fisher's sphere distribution) are listed in Table 1. For each fault, we calculated the direction of vanishing shear stress on the fault, b axis (normal to the slip axis); mean *b* values are also presented in Table 1. The symmetry of the three field measured sets (Figures 4a–4c), and the similarity between their strikes (Figure 4d) and the strikes of the digitized sets (Figure 3c), suggests the that the fourth fault set that strikes NNE (Figure 2) is oblique, normal-dextral dipping WNW. This set was not sampled due to its relative rarity.

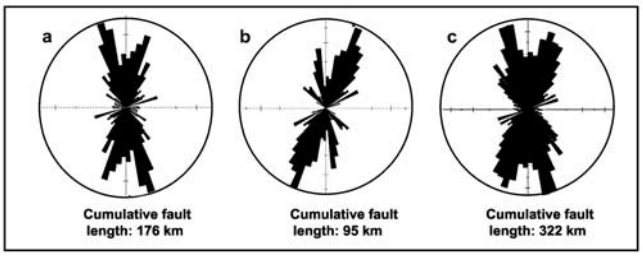

Figure 3. Strikes of the normal faults digitized in Figure 2; area weighted Rose diagrams; cumulative digitized length is marked. (a) Faults strikes of Figure 2a map. (b) Faults strikes of Figure 2b. (c) All faults strikes along WMDS belt including Figures 2a and 2b and data from *Mor* [1987]. Note dominant strike directions are 024° ± 15° and 340° ± 16°.

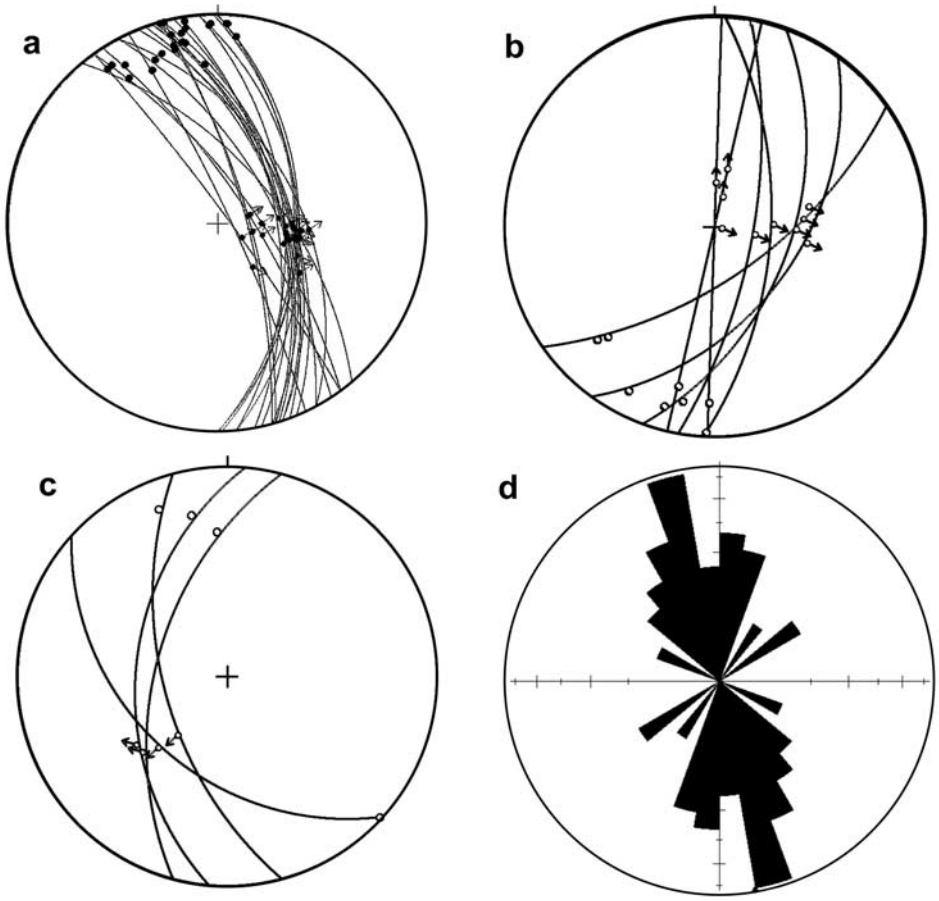

Figure 4. Directional data of large faults with slip axes measured in the field; total of 38 faults with large throw (>20 m); divided into three sets (a–c); great circles on lower hemisphere, stereographic projection; arrows- plunge direction of slip axes; small circles- b axis directions on fault surfaces; solid for downward and open for upward. (d) Strike direction of the measured faults.

[14] In summary, our field and map analyses reveal that the dominant faults distributed along the 100 km long WMDS belt are oblique-normal, with linking and cross-cutting relations that create a zigzag, orthorhombic pattern. The faults display four sets (Figure 3) with dominant strikes of 024° ± 15° (east facing) and 340° ± 16° (east facing and west facing) (Figure 3). The two east facing sets are much more common and carry much larger displacements than the west facing ones (Figure 5).

3.3. Development of Zigzag, Orthorhombic Fault System

[15] Zigzag, orthorhombic fault patterns are common in other rifts and extension regions, like the Rhine graben, the East African rift, the Rio Grande rift and parts of the Basin and Range [*Freund and Merzer*, 1976; *Illies*, 1977]. These fault patterns cannot be explained by Anderson's faulting model that predicts the development of conjugate sets (Figure 6a) rather than the observed zigzag faults (Figures 5 and 6b). *Reches* [1983] demonstrated that Anderson's model is implicitly restricted to two-dimensional strain, and derived the slip faulting model that eliminates this restriction. It was assumed by *Reches* [1983] that a region which is subjected to three-dimensional strain along its boundaries, accommodates this applies strain by slip along sets of faults (Figure 6b). It was further assumed that the faults have sufficient density and thus their cumulative slip can be modeled by a quasi-continuous strain (Figure 6b).

Table 1. Attitudes of Oblique-Normal Faults Measured in the Field (See Text)[a]

Set	N[b]	Mean Fault ± SD	Mean Slip Axis ± SD	Mean[c] b Axis ± SD
I	24	67°/070° ± 16°	64°/102° ± 10°	11°/345° ± 16°
II	10	75°/111° ± 22°	70°/074° ± 18°	−14°/17° ± 18°
III	4	56°/260° ± 23°	50°/226° ± 8°	−18°/157° ± 22°

[a]SD, spherical standard deviation (Fisher statistics).
[b]Number of field data points.
[c]Negative values indicate upward pointing axis.

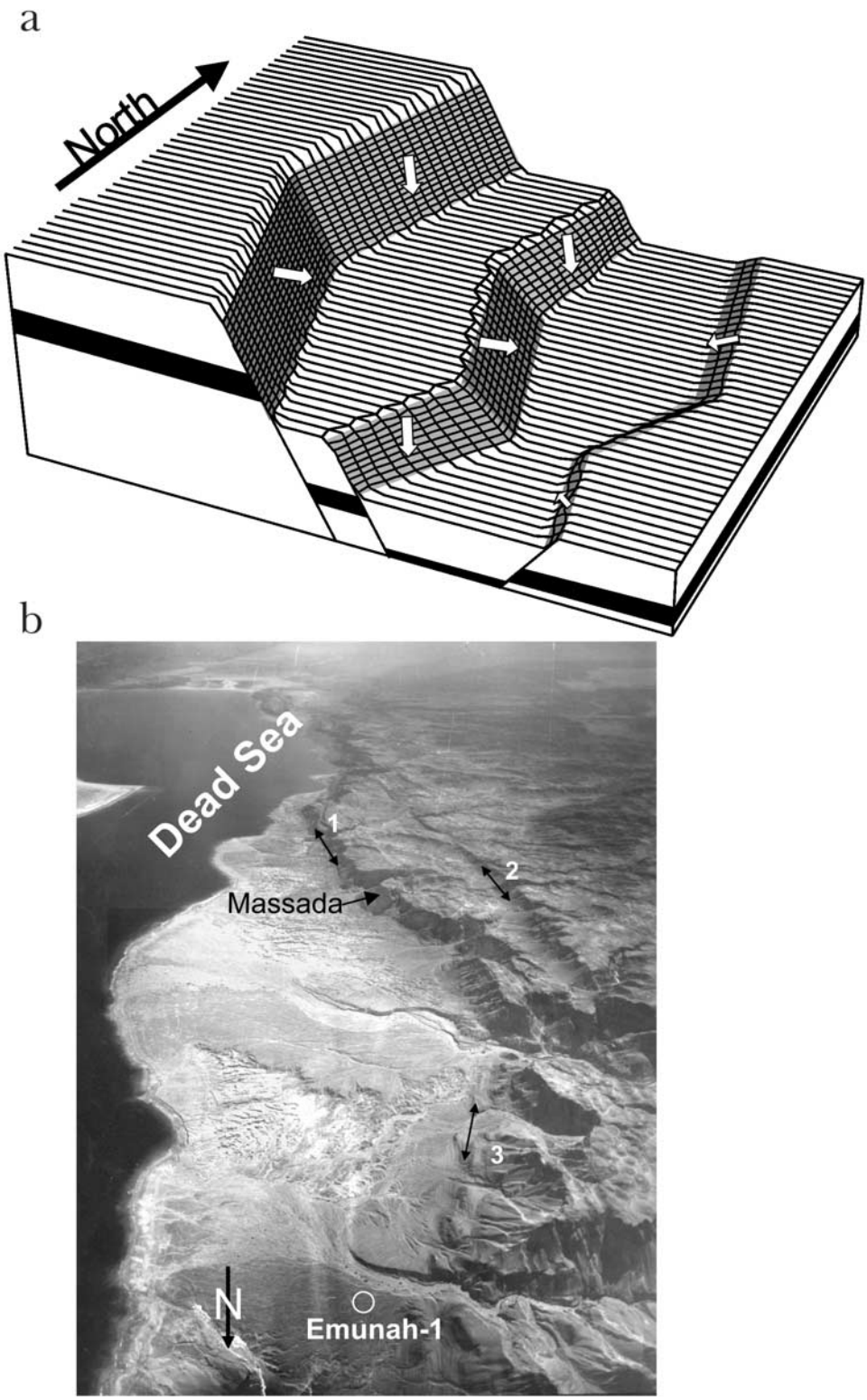

Figure 5. (a) Idealized configuration of the four dominant fault sets along the WMDS showing inclinations and slip axes on the four sets. Set orientations appear in Table 1. (b) An oblique airphoto of the central WMDS (Massada area, locations 4 and 5, Figure 1b); three prominent zigzag segments are marked (1–3). Note bright Dead Sea Group sediments (center left) and dark Cretaceous rocks (right).

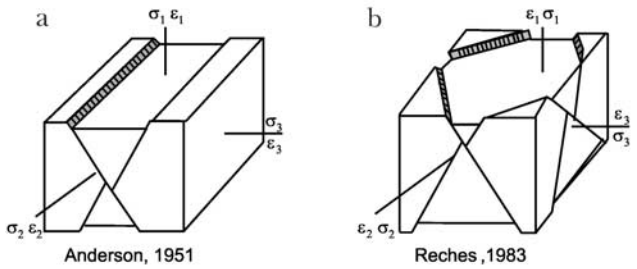

Figure 6. Predicted sets of normal faults and associated principal stress and strain axes. (a) A conjugate set after *Anderson* [1951]. (b) Four sets in 3-D strain after *Reches* [1983].

The faults obey the Coulomb friction relations and the fault sets that are activated by the applied strain are those that require the minimum mechanical energy to slip. The model predicts that zigzag, orthorhombic patterns with four sets of faults should form under a three-dimensional strain field. Further, the shape and orientations of the strain ellipsoid can be determined from the orientations the fault planes and slip axes. Several field and experimental studies have confirmed this model [*Aydin and Reches*, 1982; *Reches and Dieterich*, 1983; *Krantz*, 1989].

[16] The 3-D faulting model of *Reches* [1983] can be used to determine the regional strain in WMDS for several reasons. First, the observed zigzag pattern and the predominance of oblique-slip (Figures 4 and 5) are in qualitative agreement with the model predictions (Figure 6b). Second, there is fairly high density of the zigzag faults in WMDS (Figures 2 and 8), and the observed displacement along the exposed faults is within a limited range of a few tens to a few hundreds of meters [*Raz*, 1983; *Agnon*, 1983; *Mor*, 1987] (Figure 8). Thus the slip along the many zigzag fault segments within WMDS can be approximated as quasi-continuous extension as required by the model. Third, the observed fault sets (Figures 2 and 4) differ in orientations and style from the fault sets west and east of the WMDS, and they apparently form during a single tectonic phase (the subsidence of the Dead Sea basin; see section 7).

[17] The 3-D strain state that best fits the measured fault planes and slip axes was calculated with the 3DFAULT program (SoftStructure: Structural analysis on personal computer, available from Z. Reches at http://earth.es.huji.ac.il/reches, 1998). The results are displayed on a slip/inclination plot with the mean values of the field measured sets (Figure 7a) and the calculated best fit slip/inclination point for each of the sets. The best fit results are as follows: ε_1, maximum shortening axis is vertical; ε_2, the intermediate shortening axis is horizontal in the N-S direction; and ε_3, the minimum shortening axis is horizontal in E-W direction (Figure 7b). The slip-model considers a constant volume strain ($[\varepsilon_1 + \varepsilon_2 + \varepsilon_3 = 0$) and the shape of the strain ellipsoid is presented by the strain ratio parameter $\alpha = (\varepsilon_2 - \varepsilon_3) / (\varepsilon_1 - \varepsilon_3)$ (equivalent to the stress ratio $\phi = (\sigma_2 - \sigma_3) / (\sigma_1 - \sigma_3)$ of stress inversion analyses). For the WMDS faults we found that $\alpha \approx 0.57$ which implies that both ε_1, maximum shortening, and ε_2, intermediate shortening, are compressive, and that $\varepsilon_2 \approx 0.1\ \varepsilon_1$.

[18] The observed faults in the field (Figures 3 and 4) and their analysis (Figure 7) lack evidence of a detectable component of left-lateral displacement parallel to the Dead Sea transform. The strike-slip components of the measured oblique slip axes are about equally split between right- and left- lateral faults and therefore we interpret them to be an intrinsic part of faulting under 3-D strain field [*Reches*, 1983]. This interpretation implies strain partitioning: the sinistral strike-slip motion of the Dead Sea transform is accommodated solely along the major fault system east of WMDS (the Jordan and Arava faults; Figure 1b), whereas

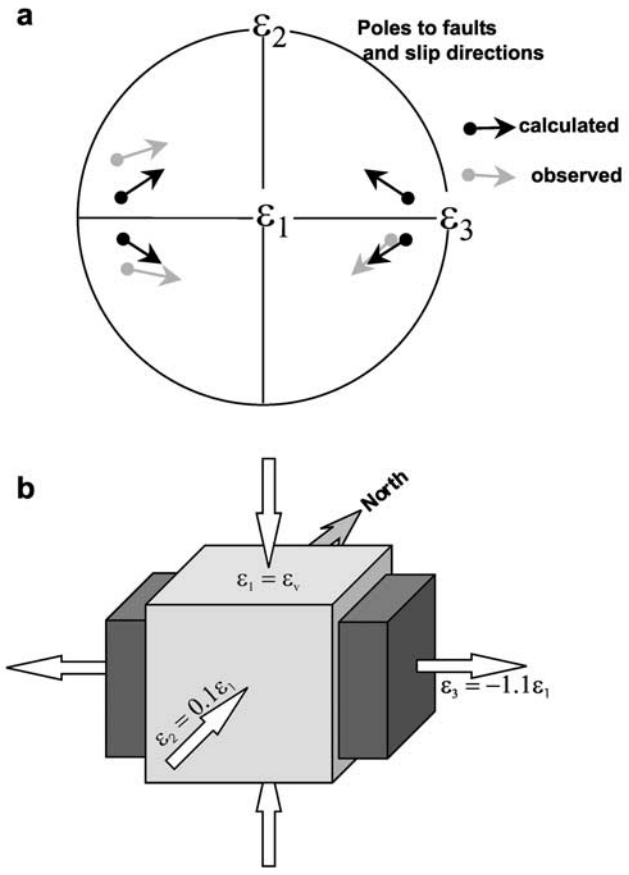

Figure 7. Best fit strain state for the measured normal faults of the WMDS calculated by 3DFAULT program of Z. Reches (SoftStructure: Structural analysis on personal computer, available at http://earth.es.huji.ac.il/reches, 1998; see text). (a) Stereographic projection showing poles of mean sets (dot) and plunge direction of slip axes (arrow) of field data (gray) and calculated sets (black). (b) Schematic representation of the strain state calculated for the measured fault data according to the *Reches* [1983] faulting model. A cube (light gray) is deformed into a box (dark gray); note the marked strain values (see text).

the WMDS fault belt itself accommodated only the horizontal extension.

4. Local-Scale Architecture: Tilted Blocks and Flexures

[19] The crosscutting zigzag faults fragmented the Upper Cretaceous sequence and generated many tilted blocks and flexures within the WMDS (Figure 8a). The common dimensions of the blocks are a few hundred meters wide and about 1–2 km long, controlled by the zigzag fault distribution. Most tilted blocks have an eastward inclination component and in the southern part of the WMDS most of the blocks dip southeastward (Figure 8a) [*Agnon*, 1983]. The latter component could have been inherited from Syrian Arc deformation (E. Aharoni, The surface and subsurface structure of southern Judean Desert, Israel, unpublished report, in Hebrew with English abstract, Hebrew University, Jerusalem, 1978). The structural throw along the tilted blocks may reach 200 m and the inclinations within the blocks are usually in the 10°–20° range (Figure 8).

[20] Narrow and elongated flexures and asymmetric folds are frequently developed above and along the WMDS faults [*Agnon*, 1983; E. Aharoni, unpublished report, The surface and subsurface structure of southern Judean Desert, Israel, in Hebrew with English abstract, Hebrew University, Jerusalem, 1978]. The steep limbs of these flexures are inclined toward the Dead Sea basin, and their widths (wavelengths) range from dozens to hundreds of meters. *Agnon* [1983] mapped several folds that are lateral extension of normal faults and which are apparently the surface expression of subsurface faults (Figure 8a).

[21] Probably the best examples of fault-flexure relations are exposed in Nahal Parsa where the cumulative throw of more than 500 m is accommodated by faulting and bending (Figure 8b). The three main blocks exposed here are separated by two large normal faults, with ~250 m throw on the western fault and at least 200 m on the eastern one. Two conspicuous asymmetric folds appear in the 220 m wide median block, and these folds are underlain by small normal faults with offset of 1–5 m (Figure 8b). A third flexure that developed east of these two folds is cut by the underlying fault. The median block itself is highly fragmented by abundant fractures, and its bending generates about 80 m of throw.

[22] It is demonstrated below that these asymmetric folds and flexures that developed above the zigzag normal faults played a central role in the architecture of the WMDS belt.

5. Small-Scale Architecture: Joints and Fractures

5.1. Field Observations

[23] We measured systematic fracture sets in 36 field stations and in one oil borehole. The field stations are located on exposures of limestone and dolostone of the Judea Group and are distributed along 50 km of the belt (locations 1–8, Figure 1b). The fractures were measured in two methods. Mapping at 1:10 scale of fractures exposed on top of subhorizontal layers (Figure 9) with complementary measurements of fracture inclinations; 21 stations were measured in this method. The maps were digitized to analyze directions, lengths and density of the sets. In 15 stations fracture orientations and frequency were measured in the scan-line method with typical line length of 30 m, and up to 120 m [*Sagy et al.*, 2001]. The measured fractures were first divided into systematic sets by using GeOrient. Then, the sets were separated into three types: joints, small faults and fractures. A set of joints was recognized by the presence of fractographic tensile features [*Bahat*, 1991]. A set of small faults was recognized by displacement or by slickenside striations.

[24] Joints are the most abundant structures within the WMDS. Most of them are restricted to individual layers, and those that crosscut packages of layers are observed primarily close to faults or along flexures [*Sagy et al.*, 2001]. The analysis is limited to systematic joint sets. The tensile nature of the joints is recognized by their fractography: concentric, rib marks, and radial (plumose and hackles) (Figure 9a). Rib marks are apparently more abundant than plumose marking in the study area.

[25] As an example, we describe the joints at Nahal Hever (location 3, Figure 1b). Figure 9b shows a map that covers about 3 m^2 of the subhorizontal top of a 0.3 m thick dolomite layer. The joint traces on the map are curved to sub-linear and many of them are segmented. In side view, the joints are generally normal to the layer and cut completely across it. Joints seldom extend into the adjacent layers or link with other joints in neighboring layers. The two joint sets recognized in Figure 9b trend 028° ± 7° and 325° ± 8°. The NNW joints are filled with secondary calcite and some of them are open up to 1 cm. For joint spacing, we used a slightly modified FSR (Fracture Spacing Ratio) parameter of *Gross* [1993]; in our calculations FSR = [(layer thickness × cumulative length of a single set] / (mapped area)]. We calculated FSR ~ 2.1 for the NNW set, which is about twice the FSR ~ 1.1 for the NNE set. The relatively higher density of the NNW set in Figure 9b is not necessarily representative of the region. The NNW set is still the dominant set in another station (Figure 9c), located 100 m westward. But in other stations (e.g., Figures 9d and 9e), located ~ 1 km further to the SE, only the NNE set is present.

[26] The analysis of all field data shows that the two sets that presented in Figure 9 belong to the dominant systematic sets of the WMDS (Figure 10). The NNE set displays highest frequency in the 020°–030° sector, and the NW-NNW set has highest frequency in the 320°–330° sector (Figure 10). In most stations, the two sets appear together, mutually crosscutting each other but with no systematic crosscutting relations between them (e.g., Figures 9b and 9c). The two sets appear in alternating dominance in the other stations. We therefore conclude that the NNW and NNE joint sets of WMDS developed during a single tectonic phase.

[27] One spectacular expression of the two dominating joint sets is large, open crevices exposed west of location 7 in Figure 2. These are dilated lineaments that are tens to hundreds meters long with apertures of up to three meters and which are open to depths of 20 m below ground surface. *Agnon* [1983] recognized their young age, as they are

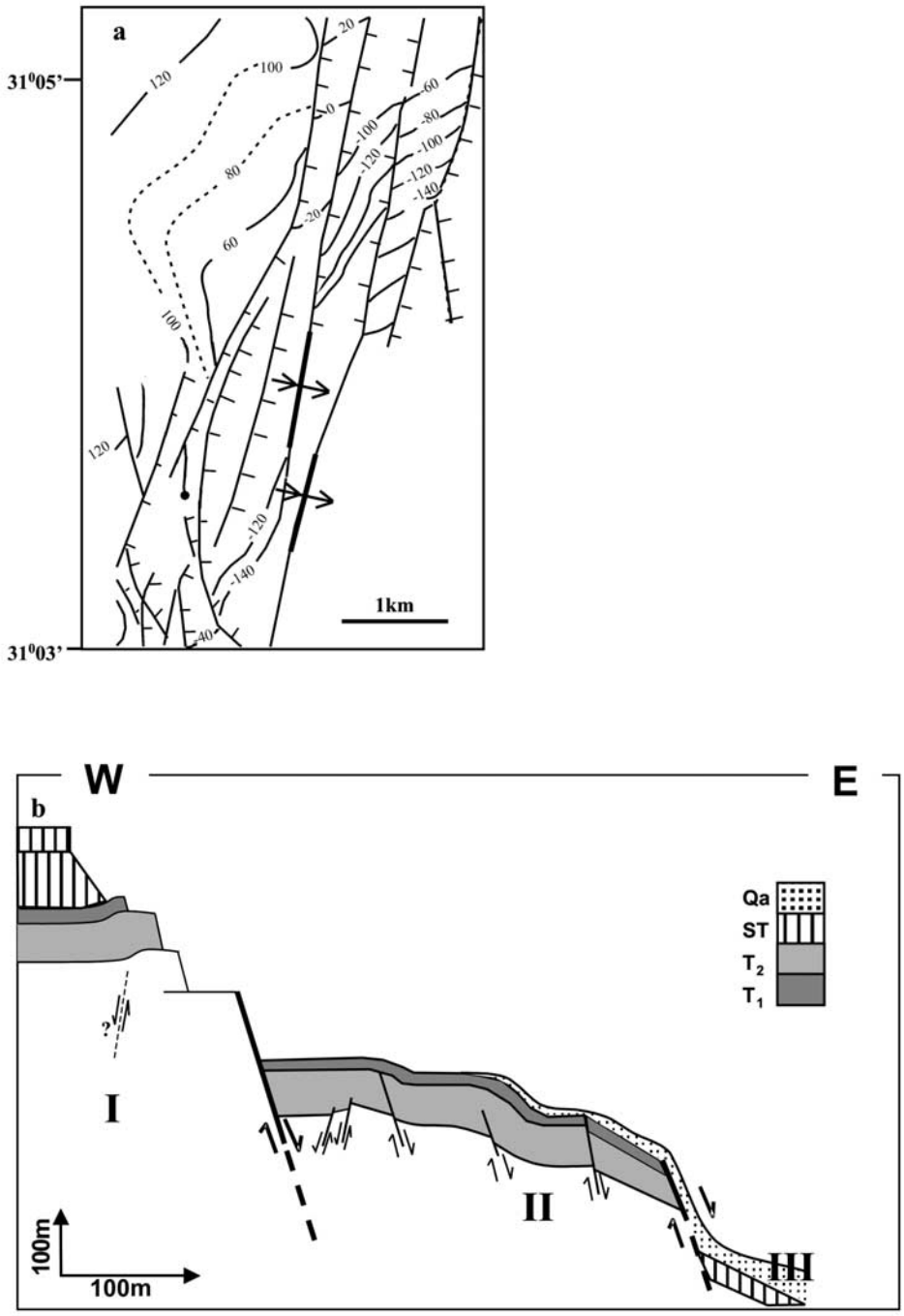

Figure 8. (a) Structural map of a portion of the WMDS (location 8, Figure 1b); modified after *Agnon* [1983]. Thin lines with bars- normal faults; thick lines with double arrows- local asymmetric folds that appear as continuation of the faults (center south); thin curves- structural contours of top Judea Group in meters above MSL. Note two southeastward tilting blocks in the east. (b) Structural section along eastern Nahal Parsa gorge (location 7, Figure 1b). Stratigraphy: t_1 and t_2- upper most units of Judea Group; sp- Mount Scopus Group; ql- Quaternary sediments. Roman numerals mark the three main blocks separated by two normal faults (thick lines); the median block (II) displays asymmetric folds underlain by small normal faults (thin lines).

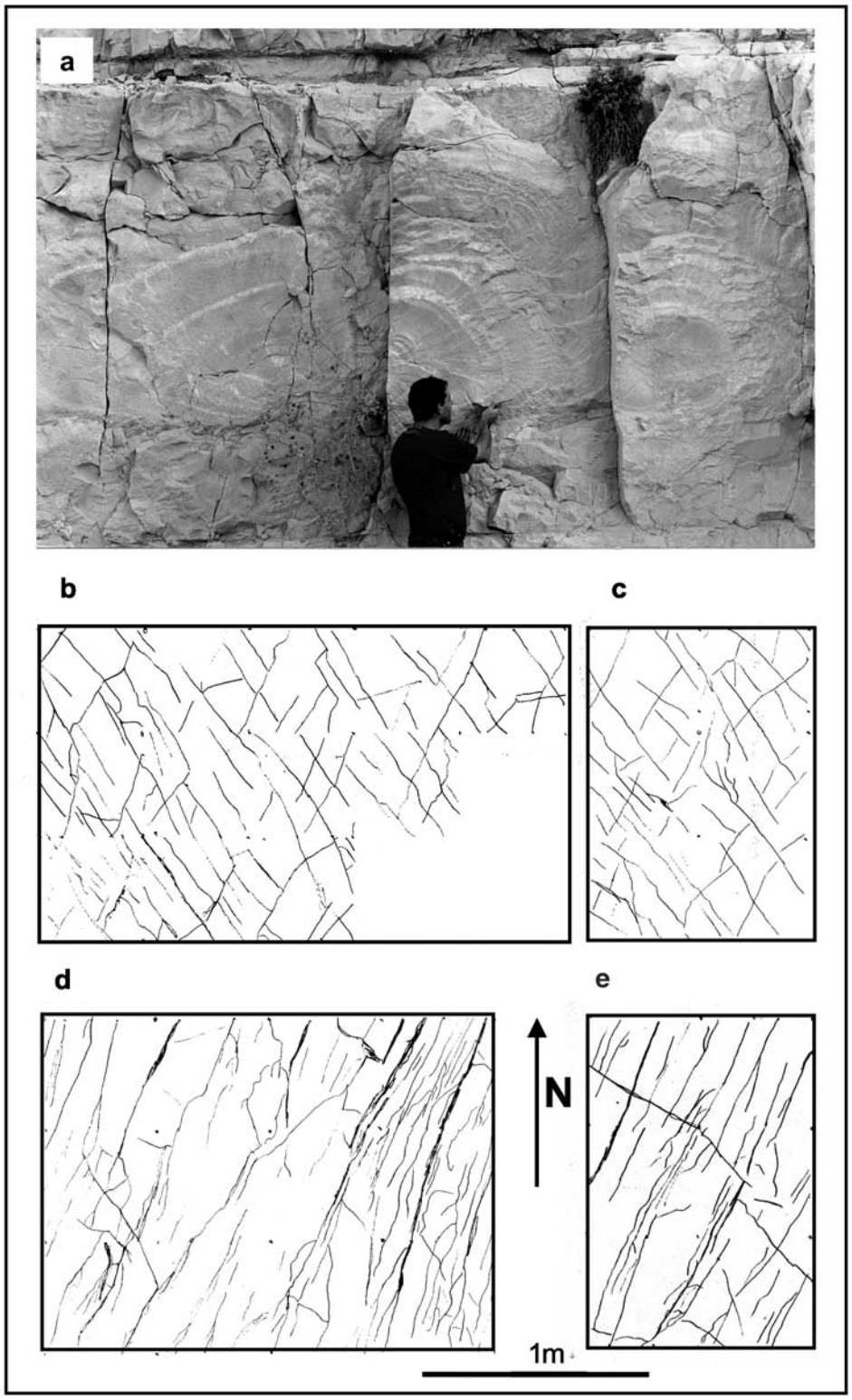

Figure 9. Observations and mapping of joints in the WMDS. (a). Fractographic features (hackles and ribs) on large joint surfaces in Nahal Mishmar (location 4, Figure 1b). (b–e) Maps of systematic joints exposed on top of subhorizontal layers at field stations in Nahal Hever; see text for description (location 3, Figure 1b).

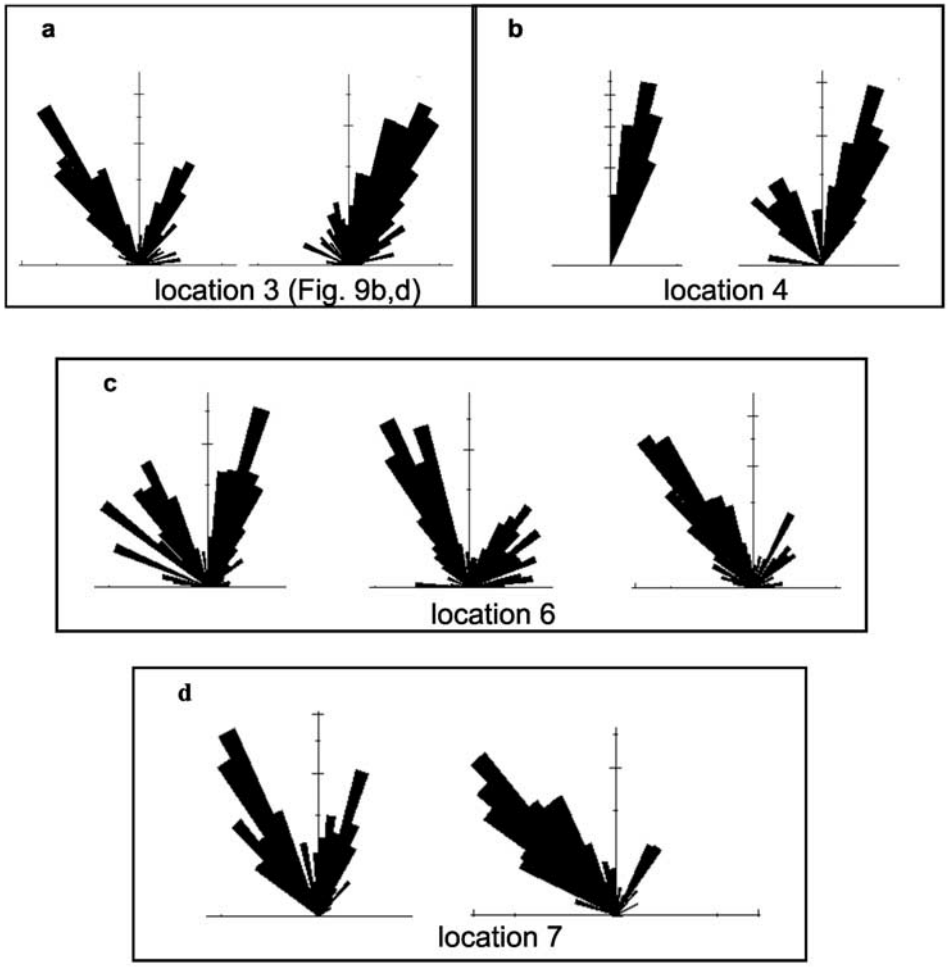

Figure 10. Strike directions of joints in nine stations along the WMDS. Projection of area weighted rose diagrams; locations in Figure 1b as follows: (a) location 3; (b) location 4; (c) location 6; and (d) location 7; the Rose diagrams of Figure 10a are of the digitized maps of Figures 9b and 9d.

associated with large displacements of 18 ka shoreline deposits. The crevices are crooked in map view and are composed of many segments with two dominating trends that parallel the presently analyzed joint sets [*Agnon*, 1983; *Arkin*, 1987; *Gilat*, 1991].

[28] The two systematic sets are not the only measured fractures. We also found small faults with slickensides and fractures of no clear mode. One group of fractures found primarily in the southwestern parts of the WMDS generally trend W-WNW and some of them carry slickenside striations. These small faults formed during the Syrian Arc folding as recognized in the entire Sinai-Israel subplate [*Eyal and Reches*, 1983]. These additional fractures form a small fraction of the regional fracture pattern and are not included in the present analysis.

5.2. Subsurface Observations

[29] Subsurface fractures were analyzed in Emunah-1 borehole that was drilled to a depth of 2850 m (location 4, Figure 1b). A few portions of the borehole were logged with CAST, Circumferential Acoustic Scanning Tool. This device measures the acoustic reflectance of borehole walls at high density, providing imaging of discontinuities, fractures and bedding surfaces, as well as borehole shape and wall damage (Figure 11). A planar surface cut by the borehole appears as a sinusoidal curve on the CAST image. We examined 564 m of available CAST images in the interval of 1400–2700 m depth, and mapped all detectable fractures by using dedicated software.

[30] The images show that the layers are subhorizontal in the logged section (Figure 11). The fractures identified on the images were qualitatively divided into four classes (A-D) according to their fit to a sinusoidal curve and their continuity on the images; class A being of highest quality. The 550 identified fractures include 107 in classes A-C; the discussion below is based on the 73 fractures of classes A and B.

[31] Three fracture sets are recognized, in azimuth convention they are 63°/068° ± 14°, 74°/259° ± 7° and 74°/312° ± 7° (Figure 11b), with strike directions of NE and

NNW (Figure 11c). These strikes are similar to the strikes of joints measured in the field (Figure 10) and to the strike directions of the large faults (Figure 3). One should note that the frequency of fractures sampled in a borehole is biased in favor of fractures that are normal to the borehole. For example, in a vertical borehole the observed spacing between parallel fractures is the ratio [(true spacing) / cos (α)], where α is the dip of the fracture set. This relation indicates poor to vanishing representation of steep to vertical fractures. We think that many vertical fractures in Emunah-1 were not detected on the CAST images but this postulate cannot be proven.

[32] We did not recognize displacement along the CAST fractures and we concluded that the mapped fractures in Emunah-1 borehole are joint or small faults. This conclusion is supported by our examination of a 10 m long continuous core collected in the borehole; we found steep fractures with no shear displacement along them [*Sagy*, 1999].

5.3. Dominant Joints in WMDS

[33] Our analysis of the fracture patterns in the field and in the subsurface revealed the following results: (1) The WMDS is dominated by two systematic sets of steep to subvertical joints with strike directions of 020°–030° (NNE set) and 320°–330° (NNW set) (Figures 9 and 10). These sets formed during a single tectonic phase in the late Cenozoic. (2) We found remarkable directional similarity between all the dominant fracture systems in WMDS: Strike directions of the two dominant joint sets measured in the exposed Cretaceous rocks (Figure 10), strike directions of the dominant fracture sets in the subsurface images in rocks as old as Triassic (Figure 11), and two strike directions of the three normal faults sets that form a zigzag pattern along the WMDS (Figure 3).

6. Structural Analysis: 3-D Association of Faults, Flexures, and Joints

6.1. Structural Implications of the Field Observations

[34] Joints, as mode I fractures, are expected to form normal to the least compressive stress axis, σ_3, with or without the contribution of pore pressure [*Engelder*, 1987]. Therefore, under a given state of stress only one set of joints should develop, and having two contemporaneous joint sets in WMDS poses some questions.

[35] Following *Zoback*'s [1992] analysis of tectonic stress fields, we consider three orders of tectonic stresses that could affect the WMDS jointing (Table 2): (1) regional-scale stresses associated with plate motion; (2) areal-scale stresses associated with major structural features, such as the western margins of the Dead Sea basin; (3) local-scale stresses associated with the perturbing stresses of large faults and folds.

[36] The stresses of the Sinai-Israel subplate since the Upper Cretaceous were separated into two stress states. One stress state is the "Syrian Arc Stress" (SAS) dominated by compressive σ_{HMAX} trending W-E to ESE-WNW; it was associated with the Syrian Arc folding and faulting [*Eyal*

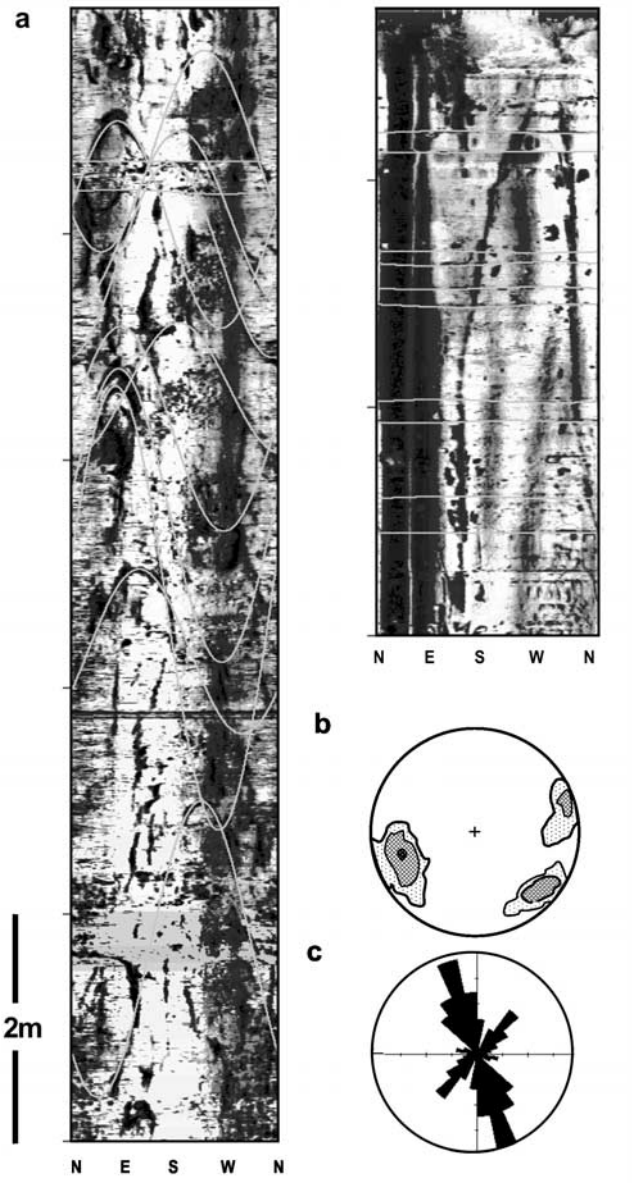

Figure 11. Subsurface fracture analysis on the CAST logs of Emunah-1 borehole (location 4, Figure 1b) (see text). (a) Two CAST images displaying an unwrapped view of the borehole wall reflectance; orientations marked at the image bottom; numbers at the right indicate layers and fractures of present analysis. Fractures appear mostly as irregular, black curves; bright, sinusoidal lines are fitted to the fracture segments and layering to determine their attitudes (see text). Note that fractures on the left image are mostly confined to the host layer, whereas a large subvertical fracture (5 m in image) crosses many layers on the right side. (b) Contoured poles to the highest quality 73 fractures determined in Emunah-1 borehole (see text). Shown 4%, 8%, and 16% contours; equal-area projection, lower hemisphere. (c) Strike directions of highest quality 73 fractures measured on the CAST images of Emunah-1.

and Reches, 1983]. The second stress state is the "Dead Sea Stress" (DSS) dominated by extensional σ_{hmin} trending ENE-WSW; it is related to the left-lateral slip along the Dead Sea transform. The expected jointing directions under these two regional stress states are WNW (by SAS) and NNW (by DSS) (Table 2). While DSS could explain the one joint set (NNW), none of the stress states could explain the NNE joints set and particularly the contemporaneous formation of these two sets (Table 2).

[37] The areal stress state of the WMDS is evaluated from the present analysis. We found that the zigzag faults formed under a 3-D strain state with ε_3, the maximum extension axis trending horizontally in E-W direction (Figure 7b). Assuming that the principal axes of strain and stress coincide, then σ_{hmin} within the WMDS trends in E-W direction, and the expected joints would be subvertical and trending N-S; this prediction does not fit the observed pattern (Table 2).

[38] The local stresses within the WMDS are related to the zigzag faults and their associated flexures that together dominate the internal structure of the belt. In the next section we explore the possibility that the observed joint sets in WMDS formed under the local stress fields due to normal faulting and associated layer flexing.

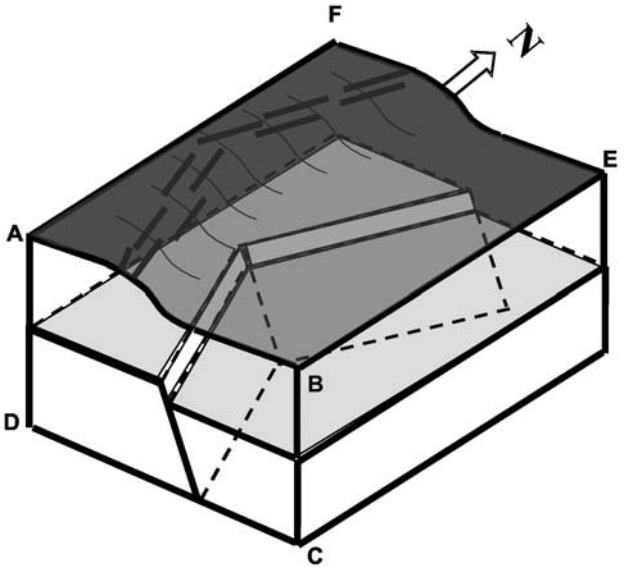

Figure 12. Idealized model for the development of two joint sets due to flexing of layers above two zigzag segments of normal faults.

6.2. Layers Flexing: Linking Normal Faults and Joints

6.2.1. Model

[39] We analyze here the mechanical relations between the dominant structures of the WMDS, zigzag faults, fault-related flexures and systematic joints. One can envision that slip along the zigzag normal faults would bend and flex the sedimentary rocks above, as manifested is several cases of transition from a normal fault at depth to a continuous flexure above (Figure 8). The slip along the normal faults and the flexing of the sedimentary layers generate a local, perturbed stress field within these layers [*Reches and Johnson*, 1978]. We postulate that the dominant joint sets formed due to this local stress field of layer bending (Figure 12). The idealized model of Figure 12 is quantified here in two steps. First, calculation of the stress fields due to slip along zigzag normal faults. Second, calculation of the stress field in a vertical profile (ABCD in Figure 12) due to slip along a normal fault underneath a layered sequence.

Table 2. Strike Directions of Observed Dominant Joint Sets and the Expected Joint Directions According to Three Orders of Stress State[a]

	Orientation (Azimuth), Deg
Observed joint sets (this work)	**010°–040°; 140°–165°**
Expected Joint Directions	
Regional-scale stress	
SAS	**90°–110°**
DSS	**165°–175°**
Areal-scale stress	
WMDS	**175°–185°**
Local-scale stress	
3-D + flexuring[b]	**020°–030°; 140°–150°**

[a]Abbreviations are as follows: SAS, Syrian arc stress [*Eyal and Reches*, 1983]; DDS, Dead Sea stress [*Eyal and Reches*, 1983]; WMDS, western margin of the Dead Sea (Figure 7).

[b]Local stresses above zigzag normal fault segments (Figures 13 and 14).

6.2.2. Calculations

[40] The horizontal stress field in the map view of our model (ABEF in Figure 12) was calculated with the DIS3D program for dislocations in linear, elastic half-space [*Erickson*, 1987]. The stress field is calculated for six planar fault segments arranged in two parallel chains with a zigzag shape. The calculations are for the areal variations of the tensile axes above buried zigzag faults that represent the general fault pattern in the WMDS; we do not attempt to solve a specific geometry. In the model, the fault segments dip 75°/070° and 75°/110°, total length of the segmented fault is 20 km, the faults extend from 2 km depth below the surface to 15 km depth, and their displacement is 1 m (Figure 13). DIS3D calculates the stress and displacement fields in three dimensions.

[41] The stress field within a vertical profile normal to one fault (ABCD in Figure 12) was calculated using the fault-fold model developed by *Reches and Zoback* [1996] (also available from Z. Reches at http://earth.es.huji.ac.il/reches, 1998). This model calculates the deformation and folding of a sequence of incompressible elastic layers above a faulted basement (Figure 14). The basement faults and the multilayer deformation are approximated by Fourier series, and the model results depend on the mechanical properties of the multilayer, the nature of the layer contacts (bonded or frictionless), thickness of the layers, the geometry of the basement faults and the slip amount. The present calculations are for two scenarios a single layer (Figure 14a), and

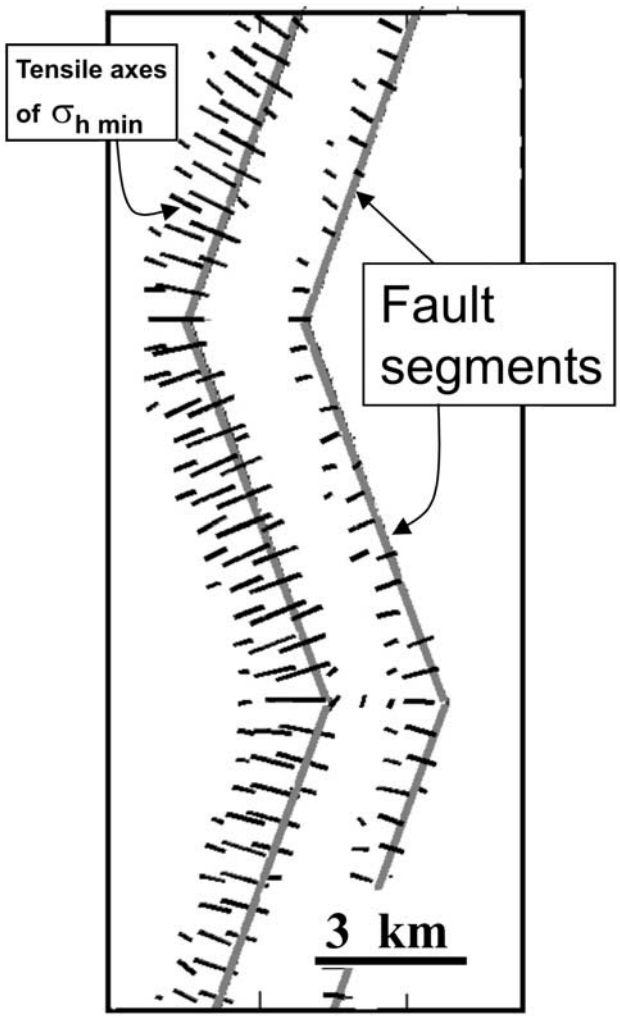

Figure 13. Calculated stress map due to slip along six fault segments in zigzag pattern. Short, black bars- orientation and relative magnitude of tensile σ_{hmin} axes; long, gray line-projection of the fault segments. See text for calculation procedure. Note that the tensile σ_{hmin} is concentrated along the faults (upper blocks) and that the tension is oriented normal to the local fault trends.

for a sequence of three layers with frictionless contacts (Figure 14b).

6.2.3. Results

[42] We used the 3-D dislocation program (DIS3D) to calculate the stress field within a horizontal surface located at 0.5 km depth, namely 1.5 km above the fault top. Figure 13 displays the orientations and magnitudes of the calculated tensile σ_{hmin} axes. The map shows that tensile stresses develop along the upper side of the faulted blocks and are arranged in belts that parallel the local fault segment. The width of the belts depends on the distance between the measuring level and the faults; for the present case (Figure 13) the width is up to 2 km. The small areas with complex local stress fields resulted from displacement singularities, are ignored here. Another important result is that the tensile stresses in the belt are oriented normal to the local strike of the fault. Thus Figure 13 indicates that (1) joints are expected to develop above a slipping fault; (2) the joints will be concentrated within belts along the upthrown side of the faults; and (3) the joints would parallel the local fault strike.

[43] In the second model we calculated the stress field in a vertical plane, trending normal to a fault segment (plane ABCD in our idealized model, Figure 12] (see also 3DFAULT program, SoftStructure: Structural analysis on personal computer, available from Z. Reches at http://earth.es.huji.ac.il/reches, 1998).

[44] The model results (Figures 14a and 14b) display the intensity of the tensile stresses (gray scale), the displacement of the layers and the orientations of the axis of maximum compression, σ_1. Four features stand out in Figure 14. First, the intensity of the tensile stresses is maximal (black) close to the buried fault and it decreases with distance from the fault. Second, tensile stresses exist within an inclined zone that, in general, forms as an upward extension of the normal fault. Third, the orientations of σ_1 axes within most of the zone of tensile stresses are subvertical. Fourth, the stress field calculated for a multilayer with free slip between the layers shows that the zone of tensile stresses is restricted to the layer immediately above the fault, whereas the upper layers are under compressive stress state.

6.2.4. Model Results and Field Observations

[45] The two models (Figures 13 and 14) are complementary and their combined results lead to the following predictions: (1) Joints are expected to develop above normal faults within belts of finite dimensions. (2) The joints are expected to be subvertical, trending parallel to the local fault segment. (3) The intensity of the jointing decreases with vertical and horizontal distance from the upper tip of the normal fault.

[46] The prediction that the dominant joint sets parallel the underlying segments of the zigzag faults can be demonstrated at several sites. Two fault sets with the same strike directions of 010°–020° were mapped in Nahal Mishmar area (location 4, Figure 1b), and a single joint set of 010°–020° direction prevails in this are (Figure 10b). Further, at this site we determined the local paleostress state by using the stress inversion method of fault-slip data [*Sagy*, 1999]. The calculations for 30 measured faults and their slip axes indicate σ_3 oriented WNW-ESE that is compatible with the directions of the local large faults and the joint set. In other sites, such as station 9, two joint directions were observed whereas only one set of faults is exposed. We suggest that the second set indicate an unexposed fault at relatively shallow depth.

[47] Another significant result of the model is the expected increase of joint density at the vertical and horizontal proximity to a fault. An excellent demonstration of this result was found in Nahal Arugot [*Sagy et al.*, 2001] (location 2, Figure 1b). At this site, the density of the NNW joint set increases systematically by more than an order of magnitude along a 120 m long traverse normal to the fault

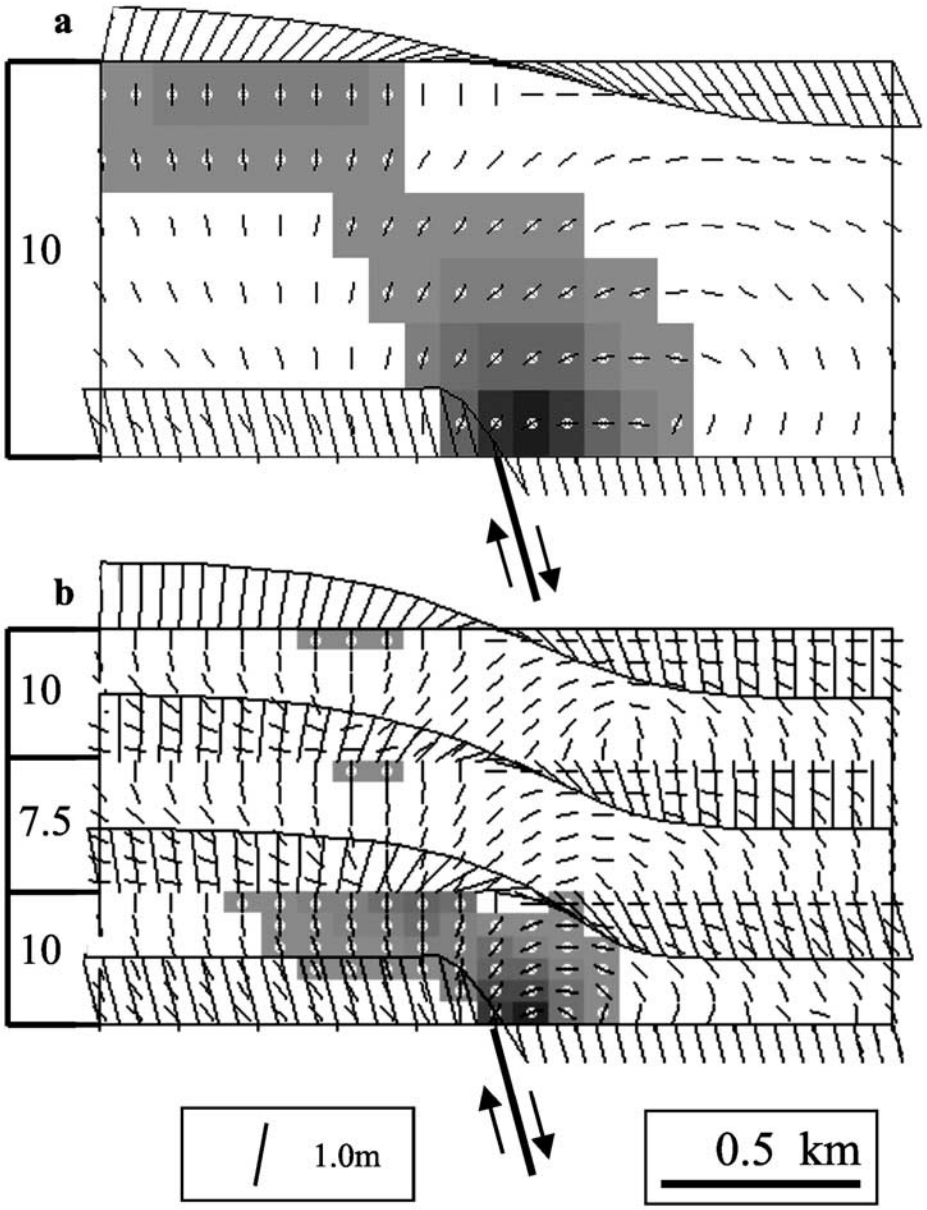

Figure 14. Stress field and deformation within a vertical section perpendicular to a normal fault. Graded gray colors- intensity of tensile stresses from highest (black) to no tension (white); short bars- local direction of σ_1 axis; layer rigidity in GPa shown on left side; displacement of base and tops of layers are shown by curved lines with connecting short lines. Calculation for 1 m slip on a 75° fault surface (see text for details). (a) Results for a single, 1 km thick layer and (b) results for three layers, 0.33 km each, with frictionless layer contacts. Note locations of high tensile stresses and orientations of tensile axes.

[*Sagy et al.*, 2001]. Increasing of joint density within the flexure above an active fault forms a damage zone that is congruent with the fault inclination (Figure 14a). This zone weakens the rocks and facilitates the localized propagation of the normal fault.

[48] The model predictions can also explain the formation of two joint sets at a given station during a single tectonic phase. Consider the following sequence of events. The local stress states alternate cyclically due to intermittent activity along faults of different attitudes (intermittent activity of faults with different orientations is known from recent seismic activity) [e.g., *Nur et al.*, 1993]. In one case, slip along a fault of set I (Figure 4a) generates local horizontal extension in ENE direction, and later slip on a crosscutting fault of set II (Figure 4b) generates, in the same rock body, local horizontal extension in ESE direction. Thus, while fault segments of all four sets move under a single areal strain state (Figure 7), they generate two alternating direc-

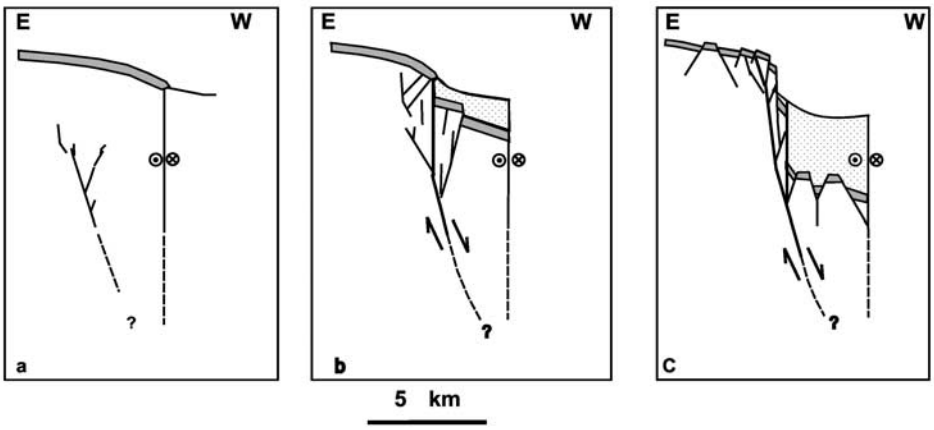

Figure 15. A schematic illustration of the major stages of the WMDS development. Gray layers- Judea Group sediments; dotted zone- basin fill sediments; thick lines- major faults. (a) Flexing of the western margins toward the subsiding pull-apart basin leading to initiation of basinward tilting and faulting at depth. (b) Localization of the normal zigzag faults, breakdown of the plate, advanced eastward tilting of the blocks and sediment filling in the basin. (c). Establishment of the zigzag fault systems and basin margins.

tions of local horizontal extension. In response to the local stresses, two joint sets form intermittently reflecting the temporal alternation of the local stress states. A rock body fractured by one set can be fractured by another set (joints or dikes), oblique to the first, under calculable stress state [*Bear et al.*, 1994]; this calculation is beyond the scope of the present study.

7. Synthesis: Structural Development of the Dead Sea Margins

7.1. Strain and Slip Partitioning Along the Dead Sea Basin

[49] While the structures within the WMDS display a coherent and distinct pattern, this pattern differs markedly from the deformation on both the west and east sides of the WMDS (Table 2). Further, the structures within the WMDS display no clear evidence for the left-lateral slip of the Dead Sea transform, even though the main left-lateral segment strand is only a few kilometers east of the study area (Figure 1b). These observations indicate that the strain of the WMDS belt was "partitioned" from the regional tectonic strain. We propose that the observed partitioning is the result of localized weakening of the WMDS belt associated with bending-driven faulting in reaction to the subsidence of the Dead Sea pull-apart. It is suggested that these processes act in the following scheme (Figure 15).

1. The left step between the two major segments of the Dead Sea transform, the Arava and Jordan segments generated the elongated and subsiding basin of the Dead Sea (Figure 1). Because of this subsidence, the western margins of the basin bent downward and eastward and extended (Figure 15a). The E-W extension and bending were observed and analyzed by *Garfunkel* [1981], *Aydin et al.* [1990], *Ben Avraham and Zoback* [1992], and *Katzman et al.* [1995]. The eastward bending affected the upper 5–10 km of the crust, perhaps rejuvenating basement, normal faults that formed in Jurassic times [*Freund et al.*, 1975].

2. The elongated bent zone generated intense localized faulting within the WMDS belt that led to the breakdown of the plate (Figure 15b). Similar breakdown and its structural consequences were extensively studied by analytical and experimental models [e.g., *Reches and Johnson*, 1978; *Withjack et al.*, 1990; *Patton et al.*, 1998]. These models predict the development of a fairly narrow fault belt, localized slip on one or two main fault zones, a lack of listric faults and a predominance of basinward inclinations of the layers (e.g., Figures 3–5 from *Patton et al.* [1998]). We note that all these features are compatible with the field observations in the WMDS, particularly the eastward tilting of the layers and the localization of more than 1 km of vertical throw along a single fault zone.

3. Our analysis of the zigzag faults revealed that the principal strain axes are oriented as $\varepsilon_1 = \varepsilon_{Vertical}$ and $\varepsilon_2 = \varepsilon_{NS}$ and $\varepsilon_3 = \varepsilon_{EW}$. As $\varepsilon_{Vertical}$ indicates shortening and according to the assumption of no volumetric change, the relative magnitudes of the principal strains are (Figure 7), $\varepsilon_{NS} \approx 0.1\ \varepsilon_{Vertical}$ and $\varepsilon_{EW} \approx -1.1\ \varepsilon_1$.

This 3-D strain state can be explained by the bending of the Sinai-Israel subplate along the WMDS into the Dead Sea basin. For sake of simplicity, we consider a rectangular plate that is 100 km long in NS direction, about 10 km wide in EW direction and about 5 km thick in the vertical direction (lower part of Figure 16b). The bending of this plate into the subsiding basin can be represented by moment M_{NS} applied on the longitudinal faces of the plate (Figure 16). Elastic plate-bending analysis indicates that under these conditions the plate will deformed into a "saddle" shape with downward bending in the EW direction and upward bending in the NS direction [e.g., *Timoshenko and Goodier*, 1970, pp. 284–289] (Figure 16b). The associated strains

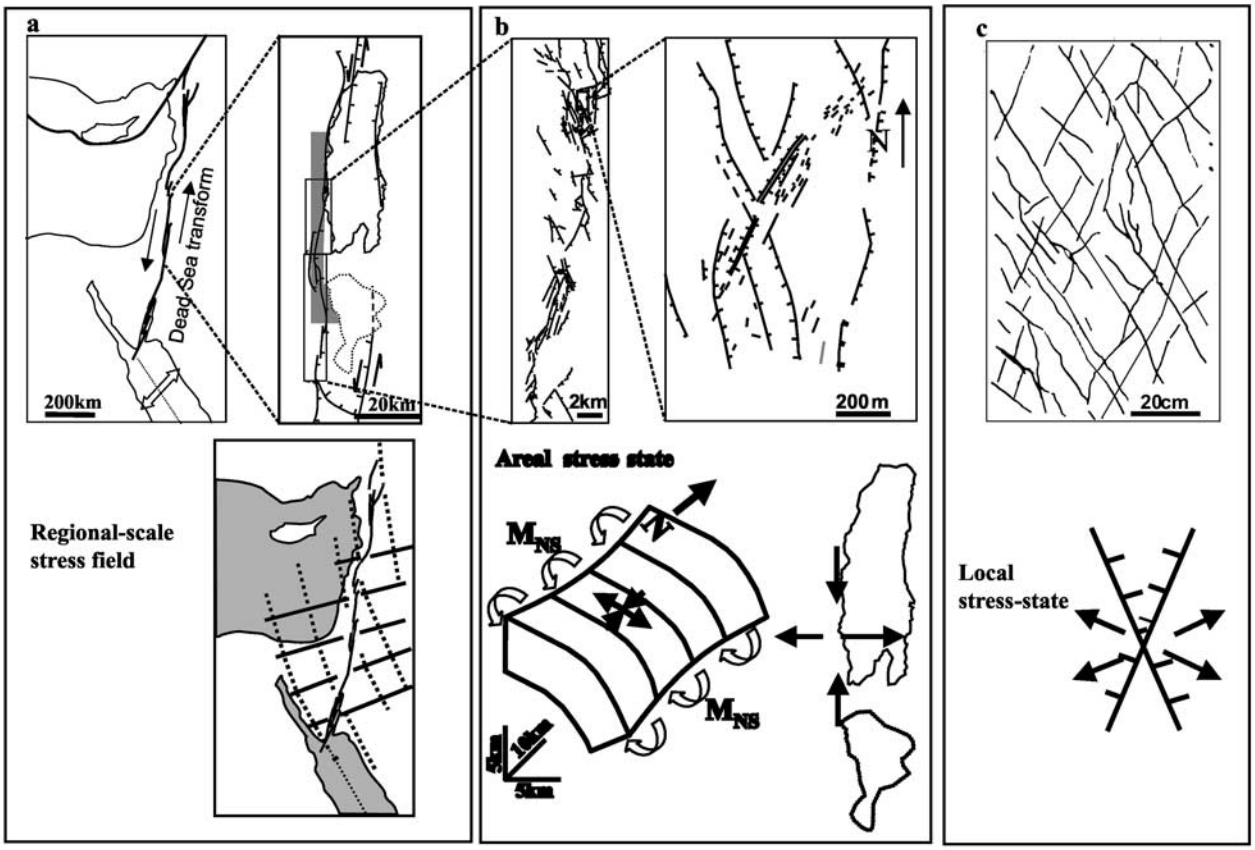

Figure 16. Structural architecture and associated stress states in the Dead Sea region. (a) Regional-scale configuration and relative motion (top left) and the Dead Sea basin (top right). Bottom: Dead Sea stress field according to *Eyal and Reches* [1983] and *Reches* [1987]; continuous lines- σ_{hmin} trajectories; dashed lines- σ_{HMAX} trajectories. (b) Areal-scale structures. Top: Oblique-normal faults from Figure 2a (left); map after *Gilat* [1991] showing faults and crevices (smooth lines) at location 7 in Figure 1b, note map scale (right). Bottom left: a simplified model of plate-bending along the WMDS under bending moment M_{NS} that leads to NS shortening and EW extension (see text). This strain state is in agreement with the 3-D analysis of the zigzag faults (Figure 7). (c) Small-scale structures (joints) that developed under the local-scale stresses associated with the flexures (Figure 8). Map of two joint sets (top); the two axes of intermittent extension directions of the local stress field generated by flexing above normal fault (bottom).

with this bending are extension in EW direction as shortening in both NS and vertical directions. These orientations are in qualitative agreement with the strain state calculated for the zigzag faults (above).

4. The 3-D strain field in the WMDS generated the dominant zigzag faults. This strain state includes a vertical ε_1, the axis of maximum shortening; and ε_3, the minimum shortening axis is horizontal in the E-W direction (Figure 7).

5. The profound weakening of the WMDS belt by the normal fault networks led to further localization of the pull-apart subsidence within this belt (Figure 15c). At the same time, the strike-slip motion has continued exclusively along the Jordan segment (Figure 1b).

7.2. Hierarchy of Structures and Stress Fields

[50] Frequently, the tectonic analyses of strain and stress fields incorporate many indicators such as slip axes along faults, directions of joints and folds [*Zoback*, 1992]. Indiscriminate projection of data collected at multiple scales could lead to chaotic patterns and prevent systematic interpretation of the tectonic history. Following Zoback's hierarchic approach of stress fields, our structural analysis of the WMDS is examined at several scales (Figure 16). The belt includes an intricate network of large zigzag oblique-normal faults with cumulative vertical motion of about 10 km (Figure 16b). This fault network includes four sets of faults in orthorhombic symmetry (Figure 16b) and it formed under 3-D strain field with maximum horizontal extension in E-W direction and N-S and vertical shortening axes (Figure 16b). The development of the zigzag fault system generated secondary systems of flexures and tilted blocks at scales of hundreds of meters (Figure 16b, top right). The occurrence of flexing and folding above normal faults were documented in extensional rifts as the Rhine Graben [*Laubscher*,

1982], and the Gulf of Suez [*Garfunkel and Bartov*, 1977; *Patton et al.*, 1994], and in lab experiments with layered samples that were subjected to faulting under uniaxial or triaxial loading [*Withjack et al.*, 1990; *Patton et al.*, 1998].

[51] In the WMDS, the local stress fields associated with the flexuring led to the fracturing, faulting and jointing of the sedimentary layers under two prevailing local and alternating tensile axes: ENE and WNW (Figure 16c). The models and laboratory experiments also predict the development of a damage zone of high intensity of fractures (joints and small faults) along normal fault. Indeed, our measurement of joint spacing showed anomalous high values of joint density at the proximity of large faults [*Sagy*, 1999; *Sagy et al*, 2001].

[52] This sequence of structural development generated the hierarchic structure depicted in Figure 16. This architecture can represent other plate boundary fracture systems as well.

[53] **Acknowledgments.** Discussions with Zvi Garfunkel, Yossi Hazor, Yossi Bartov, and Yuval Bartov are greatly appreciated. Thanks to the Israel National Oil Company for providing the CAST images of Emunah-1 borehole. Thanks to Rod Holcombe for permitting the usage the GeOrient program. The study was partly supported by the U.S.-Israel Binational Science Foundation, grant 98-135, and by the Stanford Rock Physics and Borehole Geophysics Project, 2002.

References

Agnon, A., The development of sedimentary basins and morphotectonics in the southwestern margins of the Dead Sea (in Hebrew), M.Sc. thesis, 61 pp., Hebrew Univ., Jerusalem, 1983.

Anderson, E. M., *The Dynamics of Faulting*, 206 pp., Oliver and Boyd, White Plains, N.Y., 1951.

Arbenz, J. K., Oil potential of the Dead Sea area, in *Seismic Oil Exploration*, *Rep., 84/111*, 44 pp., Sismica, Tel Aviv, 1984.

Arkin, Y., Large-scale tensional features along the Dead Sea-Jordan Rift valley, *Tectonophysics*, *165*, 143–154, 1987.

Aydin, A., and Z. Reches, Number and orientation of fault sets in the field and in experiments, *Geology*, *10*, 107–112, 1982.

Aydin, A., R. A. Schultz, and D. Campagna, Fault-normal dilation in pull-apart basins: Implications for relationship between strike-slip faults and volcanic activity, *Ann. Tectonicae*, *4*, 45–52, 1990.

Bahat, D., *Tectono-Fractography*, 354 pp., Springer-Verlag, New York, 1991.

Bartov, Y., The geology of Lisan formation in Massada plain and the Lisan peninsula, M.Sc. thesis, 61 pp., Hebrew Univ., Jerusalem (in Hebrew with English abstract), 1999.

Bear, G., M. Beyth, and Z. Reches, Dikes emplaced into fractured basement, Timna igneous complex, Israel, *J. Geophys. Res.*, *99*, 24,039–24,050, 1994.

Ben Avraham, Z., and M. D. Zoback, Transform-normal extension and asymmetric basins: An alternative to pull-apart models, *Geology*, *20*, 423–426, 1992.

Engelder, T., Joints and shear fractures in rock, in *Fracture Mechanics of Rock*, edited by B. K. Atkinson, pp. 27–69, Academic, San Diego, Calif., 1987.

Erickson, L., User's manual for DIS3D, a three-dimensional dislocation program with application to faulting in the Earth, 167 pp., Applied Earth Sci., Stanford Univ., Calif., 1987.

Eyal, Y., and Z. Reches, Tectonic analysis of the Dead Sea Rift region since the Late-Cretaceous based on mesostructures, *Tectonics*, *2*, 167–185, 1983.

Freund, R., and A. M. Merzer, The formation of rift valleys and their zigzag fault patterns, *Geol. Mag.*, *113*, 561–568, 1976.

Freund, R., M. Goldberg, T. Weissbrod, Y. Druckman, and B. Derin, The Triassic-Jurassic structure of Israel and its relation to the origin of the eastern Mediterranean, *Bull. Geol. Surv. Isr.*, *65*, 26, 1975.

Gardosh, M., Z. Reches, and Z. Garfunkel, Holocene tectonic deformation along the western margins of the Dead Sea, *Tectonophysics*, *180*, 123–137, 1990.

Gardosh, M., E. Kashai, S. Salhov, H. Shulman, and E. Tannenbaum, Hydrocarbon exploration in the southern Dead Sea area, in *The Dead Sea, The Lake and Its Setting*, edited by T. M. Niemi, Z. Ben Avraham, and J. R. Gat, pp. 57–72, Oxford Univ. Press, New York, 1997.

Garfunkel, Z., Internal structure of the Dead Sea leaky transform (rift) in relation to plate kinematics, *Tectonophysics*, *80*, 81–108, 1981.

Garfunkel, Z., The history and formation of the Dead Sea basin, in *The Dead Sea, The Lake and Its Setting*, edited by T. M. Niemi, Z. Ben Avraham, and J. R. Gat, pp. 36–56, Oxford Univ. Press, New York, 1997.

Garfunkel, Z., Constrains on the origin and history of the eastern Mediterranean Basin, *Tectonophysics*, *298*, 5–35, 1998.

Garfunkel, Z., and Y. Bartov, The tectonics of the Suez Rift, *Bull. Geol. Surv. Isr.*, *71*, 44, 1977.

Gilat, A., Oversized U-shaped canyon development at the edge of rotating blocks due to wrench faulting on margins of the Dead Sea graben, *Terra Nova*, *3*, 638–647, 1991.

Ginzburg, A., and Z. Ben Avraham, A seismic refraction study of the north basin of the Dead Sea, Israel, *Geophys. Res. Lett.*, *24*, 2063–2066, 1997.

Gross, M. R., The origin and spacing of cross joints: Examples from the Monterey Formation, Santa Barbara coastline, California, *J. Struct. Geol.*, *15*, 737–751, 1993.

Illies, J. H., Ancient and recent rifting in the Rhine graben, in *Fault Tectonics in Europe, N. W.*, edited by R. T. C. Frost and A. J. Dikkers, *Geol. Mijnbouw*, *56*, 329–350, 1977.

Joffe, S., and Z. Garfunkel, Plate kinematics of the circum Red Sea: A re-evaluation, *Tectonophysics*, *141*, 5–22, 1986.

Kashai, E. L., and P. F. Croker, Structural geometry and evolution of the Dead Sea-Jordan rift system as deduced from new subsurface data, *Tectonophysics*, *141*, 33–60, 1987.

Katzman, R., U. S. Ten Brink, and J. Lin, Three Dimensional modeling of pull-apart basins: Implication for the tectonics of the Dead Sea basin, *J. Geophys. Res.*, *100*, 6295–6312, 1995.

Krantz, R. W., Orthorhombic fault patterns: The odd axis model and slip vector orientations, *Tectonics*, *8*, 483–495, 1989.

Laubscher, H. P., The southeastern extremity of the Rhine Graben; kinematic and dynamic problem, *Eclogae Geol. Helv.*, *75*, 101–116, 1982.

Mor, U., The geology of Judea Desert in Nahal Darga area (in Hebrew with English abstract), M.Sc. thesis, 112 pp., Hebrew Univ., Jerusalem, 1987.

Neev, D., and J. K. Hall, Geophysical investigations in the Dead Sea, *Sediment. Geol.*, *23*, 209–238, 1979.

Nur, A., H. Ron, and G. Beroza, The nature of the Landers-Mojave earthquake line, *Science*, *261*, 201–203, 1993.

Patton, T. L., A. R. Moustafa, R. A. Nelson, and A. S. Abdine, Tectonic evolution and structural setting of the Suez Rift, *AAPG Mem.*, *59*, 9–55, 1994.

Patton, T. L., J. M. Logan, and M. Friedman, Experimentally generated normal faults in single-layer and multilayer limestone specimens at confining pressure, *Tectonophysics*, *295*, 53–77, 1998.

Quennell, A. M., Tectonics of the Dead Sea rift, *Int. Geol.*, 385–405, 1959.

Raz, E., The geology of Judea Desert, En-Gedi area (in Hebrew with English abstract), M.Sc. thesis, 112 pp., Hebrew Univ., Jerusalem, 1983.

Reches, Z., Faulting of rocks in three-dimensional strain field, II, Theoretical analysis, *Tectonophysics*, *95*, 133–156, 1983.

Reches, Z., Mechanical aspects of pull-apart basins and push-up swells with applications to the Dead Sea Transform, *Tectonophysics*, *141*, 75–88, 1987.

Reches, Z., and J. Dieterich, Faulting of rocks in three-dimensional strain field, I, Failure of rocks in polyaxial, servo-control experiments, *Tectonophysics*, *95*, 111–132, 1983.

Reches, Z., and A. M. Johnson, Development of monoclines, part II, Theoretical analysis of monoclines, *Mem. Geol. Soc. Am.*, *151*, 273–311, 1978.

Reches, Z., and M. D. Zoback, Mechanical modeling of a fault-fold system, with application to the earthquake, in *The Loma Prieta, California, Earthquake of October 17, 1989: Main-Shock Characteristics*, edited by P. Spudich, *U. S. Geol. Surv. Prof. Pap.*, A183–A194, 1996.

Sagy, A., Jointing and faulting processes along the western margin of the Dead Sea basin (in Hebrew with English abstract), M.Sc. thesis, 45 pp., Hebrew Univ., Jerusalem, 1999.

Sagy, A., Z. Reches, and I. Roman, Dynamic fracturing: Field and experimental observations, *J. Struct. Geol.*, *23*, 1223–1239, 2001.

Tannenbaum, E., Researches in the geochemistry of oils and asphalts in the Dead Sea area (in Hebrew with English abstract), Ph.D. dissertation, Hebrew Univ., Jerusalem, 1983.

Timoshenko, S. P., and J. N. Goodier, *Theory of Elasticity*, 567 pp., McGraw-Hill, New York, 1970.

Withjack, M. O., J. Olson, and E. Peterson, Experimental models of extensional forced folds, *AAPG Bull.*, *74*, 1038–1054, 1990.

Zoback, M. L., First- and second-order patterns of stress in the lithosphere: The World Stress Map Project, *J. Geophys. Res.*, *97*, 11,703–11,728, 1992.

A. Agnon, Z. Reches, and A. Sagy, Institute of Earth Sciences, Hebrew University, Jerusalem, 91904, Israel. (amotz@cc.huji.ac.il; reches@earth.es.huji.ac.il; sagy@vms.huji.ac.il)